Appl Phys A (2012) 107:49–54
DOI 10.1007/s00339-011-6736-y

Applied Physics A
Materials Science & Processing

INVITED PAPER

Optically tunable plasmonic color filters

Y.J. Liu · G.Y. Si · E.S.P. Leong · B. Wang · A.J. Danner · X.C. Yuan · J.H. Teng

Received: 11 July 2011 / Accepted: 8 December 2011 / Published online: 22 December 2011

Abstract We fabricated sub-wavelength patterned gold plasmonic nanostructures on a quartz substrate through the focused ion beam (FIB) technique. The perforated gold film demonstrated optical transmission peaks in the visible range, which therefore can be used as a plasmonic color filter. Furthermore, by integrating a layer of photoresponsive liquid crystals (LCs) with the gold nanostructure to form a hybrid system, we observed a red-shift of transmission peak wavelength. More importantly, the peak intensity can be further enhanced more than 10% in transmittance due to the refractive index match of the media on both sides of it. By optically pumping the hybrid system using a UV light, nematic−isotropic phase transition of the LCs was achieved, thus changing the effective refractive index experienced by the impinging light. Due to the refractive index change, the transmission peak intensity was modulated accordingly. As a result, an optically tunable plasmonic color filter was achieved. This kind of color filters could be potentially applied to many applications, such as complementary metal-oxide-semiconductor (CMOS) image sensors, liquid crystal display devices, light emitting diodes, etc.

Y.J. Liu · E.S.P. Leong · B. Wang · J.H. Teng (✉)
Institute of Materials Research and Engineering, Agency for Science Technology and Research (A*STAR), 3 Research Link, Singapore 117602, Singapore
e-mail: jh-teng@imre.a-star.edu.sg

G.Y. Si · A.J. Danner
Department of Electrical and Computer Engineering, National University of Singapore, 4 Engineering Drive 3, Singapore 117576, Singapore

X.C. Yuan
Institute of Modern Optics, Key Laboratory of Optoelectronic Information Science & Technology, Ministry of Education of China, Nankai University, Tianjin 300071, China

1 Introduction

Nowadays, color filters are a crucial component for various applications, such as digital cameras, complementary metal-oxide-semiconductor (CMOS) image sensors, liquid crystal displays, and light emitting diodes. Current research on color filtering is focused on developing smaller, faster, smarter, and lower-power designs. Plasmonic color filters are promising to meet these challenges due to the nature of surface plasmons (SPs). SPs are essentially charge density waves generated by the coupling of light to the collective oscillation of electrons at the metal/dielectric interface [1]. Colloidal gold and silver have been used to color glass of intense shades of yellow, red, or mauve since ancient Roman times, depending on the concentration of the two metals. An excellent example is the famous Lycurgus Cup in the British Museum, dated 4th century AD. Recently, by precisely engineering plasmonic nanostructures, such as nanohole or nanodisk arrays, coupling between photons and plasmons can be efficiently controlled at subwavelength scale [2–5], thus opening a platform for many applications. Thus far, considerable efforts have been made to explore different plasmonic nanostructures to filter colors by tuning the resonant transmission peak at the visible range, such as nanohole array [6, 7] and nanoslits combined with period grooves [8]. In addition, the metal-insulator-metal (MIM) structures have [9–11] also shown color filtering effect. However, such filters usually have low transmission due to the high loss of metals and relatively broad passing bands, which do not satisfy the requirement for the multiband spectral imaging. Therefore, it is highly desirable to improve the performance of plasmonic color filters for their practical applications.

One strategy is to explore new structures to achieve both high transmission and narrow passing band. In this paper, we shall investigate new plasmonic nanostructures and explore

their use for color filters. Furthermore, by applying a layer of photoresponsive liquid crystals (LCs) onto the gold nanostructure, the peak intensity can be further enhanced more than 10% in transmittance. By optically pumping the hybrid system, the transmittance can be efficiently modulated.

2 Experimental

2.1 Plasmonic nanostructures fabrication

In our experiment, the noble metal, Au, was selected for the fabrication of plasmonic nanostructures. In brief, a Ti adhesion layer (3 nm) and an Au layer (110 nm) were subsequently deposited on a quartz substrate by electron-beam evaporation (EDWARDS Auto 306 Turbo E-beam Evaporator). Based on an improved focused ion beam (FIB) (FIB 200, FEI Company) patterning method, we then fabricated dense plasmonic crystal arrays with varying lattices. To minimize redeposition effects, all patterns were milled in parallel instead of serial. A probe current of 70 pA was applied with a 30 kV acceleration voltage during the milling process. Figure 1 shows the schematic drawing of a typical pattern fabricated in this work using FIB lithography. Lattice shape was controlled by varying ring gap apertures. By aligning coaxial ring-like structures, one can remove the parts between coaxial structures simply, leaving dense arrays with different lattice shapes. Such an improved FIB patterning method provides easy fabrication of one-/two-dimensional (1D/2D) metallic patterns with higher aspect ratios than the standard electron beam lithography (EBL), since there is no limitation of selectivity issues. Moreover, one can precisely control the geometry and the overlapping areas by varying inner and outer radii of individual nanorods and changing the distance between nanorods. Therefore, the entire process is highly accurate and monolithic.

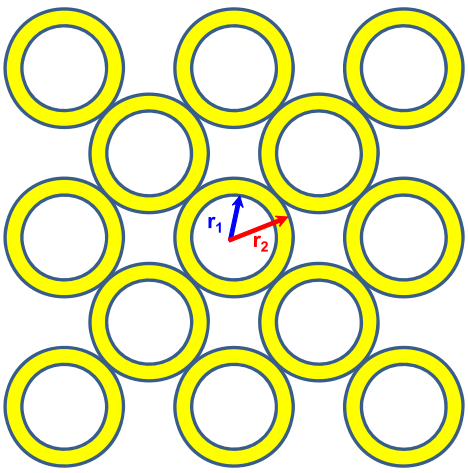

Fig. 1 Schematic diagram of the FIB lithography method for 2-D plasmonic crystal fabrication based on nanoring patterning. The inner and outer radii of each individual nanorod are labeled as r_1 and r_2, respectively

2.2 Liquid crystal infiltration

To apply a LC layer on the plasmonic nanostructure, a cell was formed by assembling two substrates: one is a quartz substrate with plasmonic nanostructures and the other one was an indium-tin-oxide (ITO) glass substrate coated a rubbed polyimide (PI) alignment layer. The cell thickness was controlled to be ~7 μm using the polystyrene microbeads. The LC material used in our experiments consisted of 87.3 wt% nematic LC, E7 (Merck), and 12.7 wt% photochromic LC, 4-butyl-4-methyoxyazobenzene (BMAB), which were mechanically mixed at an elevated temperature of 70°C to form a homogenous mixture. The LC E7 serves as a host material, which has an ordinary refractive index of $n_o = 1.521$ and an extraordinary refractive index of $n_e = 1.746$, giving a birefringence of $\Delta n = 0.225$ (all at $\lambda = 589$ nm). BMAB is an azobenzene derivative, and it possesses an alkoxy substituent and a butyl group at the para positions of the azobenzene. BMAB has a liquid crystalline behavior with a nematic–isotropic (N–I) phase transition temperature at $T_{NI}(\text{BMAB}) = 45°\text{C}$. The homogeneous mixture was infiltrated into the LC cell by a capillary action. After infiltration of LCs, a roughly homogeneous alignment of LCs was expected, i.e., LC molecules aligned parallel to the substrates, due to the fact that the alignment layer on the ITO glass substrate caused a preferred alignment across the cell through the van der Waals force between LC molecules.

2.3 Spectra measurement

Optical transmission spectra were measured with an unpolarized probe light beam using a UV-Vis-NIR microspectrophotometer (CRAIC QDI 2010™). Figure 2 shows the schematic drawing of the experimental setup for characterization of the hybrid system. The probe light beam was focused to have a detecting area of 7.1 × 7.1 μm^2 using a 36× objective lens combined with a variable aperture. The dynamic spectral change was achieved when the hybrid system was subject to a flood exposure using a UV light source (ELC-410).

3 Results and discussion

A set of field emission scanning electron microscope (FE-SEM) images of the fabricated Au plasmonic nanostructures array are shown in Fig. 3 with varied inner and outer radii. The whole working area of each pattern is 10 × 10 μm^2. From Fig. 3, kaleidoscopic patterns can be generated by

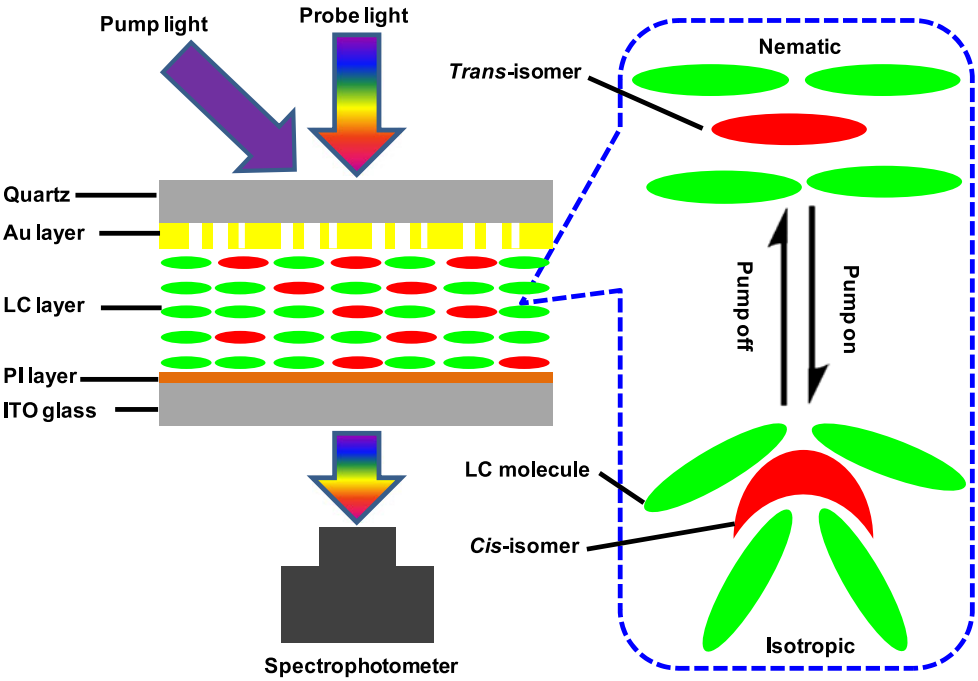

Fig. 2 Schematic of the experimental setup for characterization of the hybrid system. The enlarged part shows the reversible N–I phase transition induced by the *trans-cis* photoisomerization of the photochromic LCs

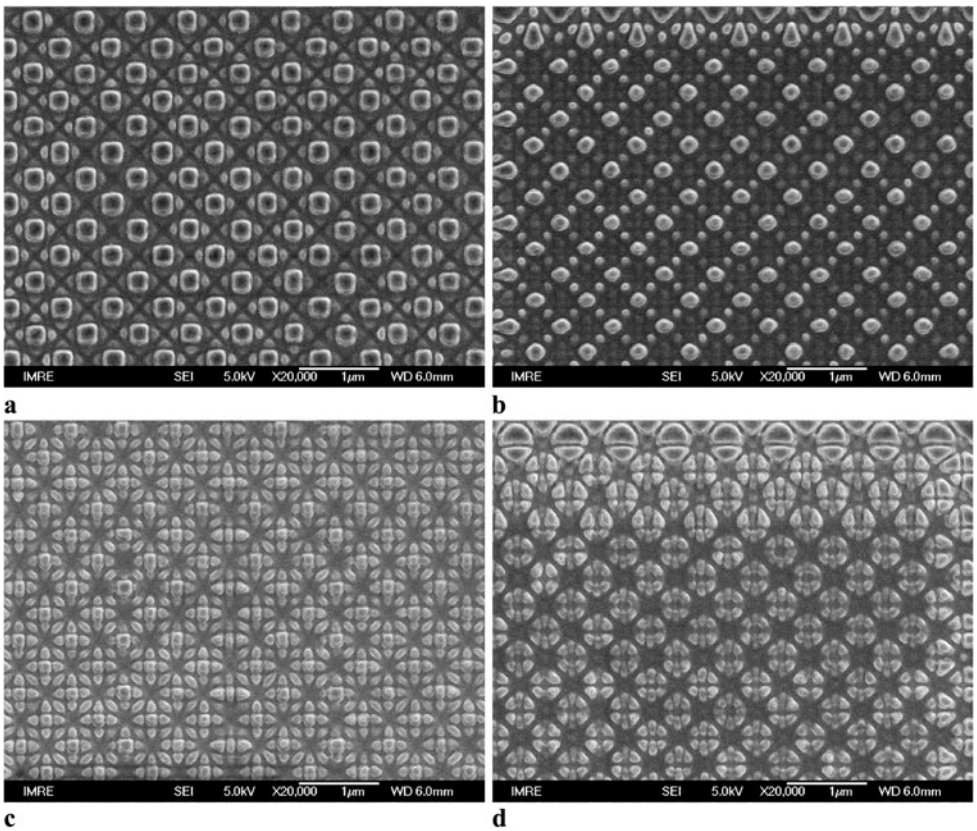

Fig. 3 SEM images showing the Au plasmonic nanostructures with varied inner and outer radii: (**a**) $r_1 = 0.45$ μm, $r_2 = 0.46$ μm; (**b**) $r_1 = 0.55$ μm, $r_2 = 0.56$ μm; (**c**) $r_1 = 0.70$ μm, $r_2 = 0.71$ μm; (**d**) $r_1 = 0.90$ μm, $r_2 = 0.92$ μm

varying the inner and outer radii, thus causing a significant effect on the optical transmission of these nanostructures due to the nanostructure geometry-induced photon-plasmon-photon conversion process.

By integrating a layer of photoresponsive LCs with the Au plasmonic nanostructures, a hybrid system was formed. Meanwhile, an optically active functionality was incorporated in this hybrid system. As known, a distinct advantage

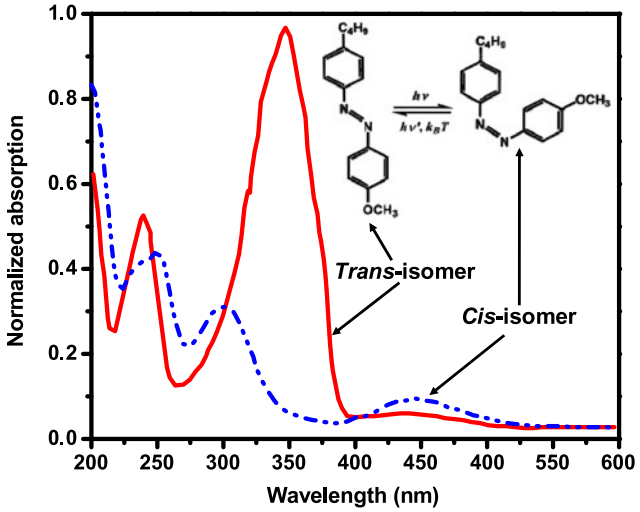

Fig. 4 The trans-cis isomerization of BMAB under the UV flood exposure. The inset shows the chemical structure of a BMAB molecule and its reversible trans-cis isomerization

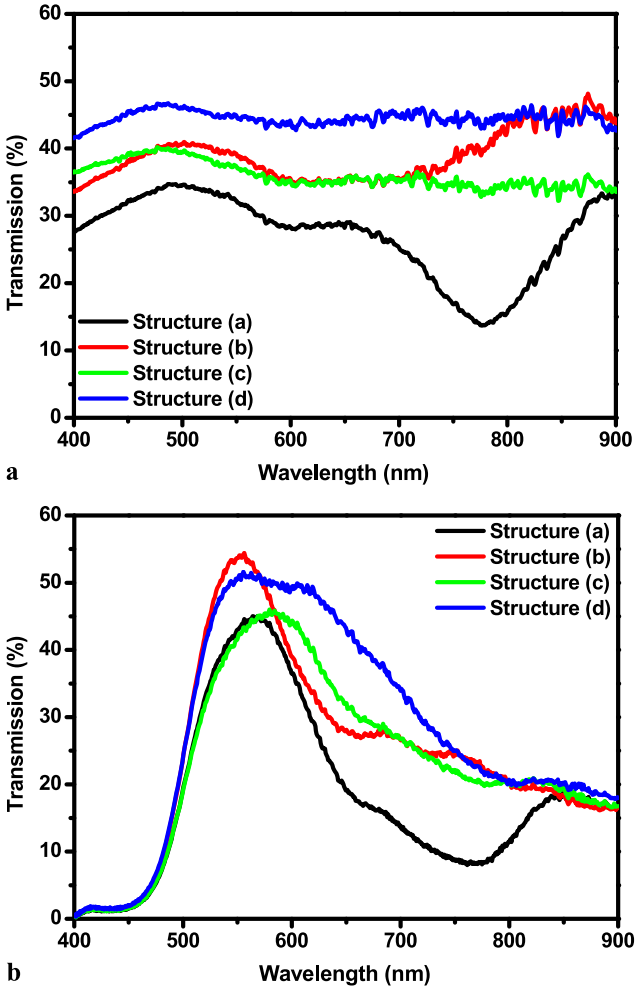

Fig. 5 Transmission spectra of the Au plasmonic nanostructures before (**a**) and after (**b**) infiltration of the photoresponsive LCs for normally incident unpolarized light

of azobenzene and azobenzene derivatives is that they can undergo a reversible photoisomerization between the *trans* (rodlike shape) and the *cis* (bent shape) molecular forms upon irradiation with UV or visible light [12, 13]. Figure 4 shows the measured absorption spectra of the *trans* and the *cis* forms of the BMAB molecules. The *trans*-isomer has a main absorption band in the UV around 350 nm (π–π^* molecular transition), whereas the *cis*-isomer has an absorption peak in the visible around 450 nm (n–π^* molecular transition). The *trans*-isomer, which is the thermally stable ground state, can transform into the *cis*-isomer by absorbing UV light. Under visible light irradiation or thermal isomerisation, the *cis*-isomer can return to the *trans*-isomer form [14], making the hybrid system highly reversible and reproducible.

The transmission spectra of the Au plasmonic nanostructures before and after infiltration of the photoresponsive LCs were recorded with normally incident light, respectively, as shown in Figs. 5(a) and 5(b). From Fig. 5(a), it is clear that all the Au nanostructures show a transmission peak near 500 nm, which is coincident with transmission peak at ∼500 nm for the continuous Au film. As known, for continuous Au films, the transmission peak arises from the electrons transition and recombination between the filled d-bands and the Fermi level in conduction band [15–17] and the transmittance is strongly dependent on the film thickness. For the continuous Au film with the thickness of 110 nm in our experiments, the peak transmittance was less than 10%. However, for all the Au plasmonic nanostructures, the peak transmittance is larger than 30%, which could be attributed to SP-enhanced transmission as well as the reduction of the metal quantity. After the infiltration, the transmission peak has a red-shift. More importantly, much more pronounced transmission peaks appear for all the Au plasmonic nanostructures and their peak intensities are significantly enhanced compared to the bare Au nanostructures. The large enhancement can be attributed to the application of the photoresponsive LC layer to the plasmonic nanostructures, which leads to an index matching of the media on both sides of it, thus further boosting the optical transmission [18]. Table 1 summarizes the measured peak position and transmittance of each plasmonic nanostructure before and after infiltration of the photoresponsive LCs. From Table 1, structure (c) gives the largest red-shift (103 nm), while structure (b) provides the largest enhancement of peak transmittance (13.4%). We believe that the interaction between the LC alignment and the plasmonic nanostructure's geometry and topography have a determinative role on the LCs' alignment at the LC/nanostructure interface, thus affecting the effective refractive index experienced by the impinging light and the subsequent peak shift and enhancement.

Table 1 The measured peak position and transmittance of each plasmonic nanostructure before and after infiltration of the photoresponsive LCs

	Before infiltration		After infiltration	
	Peak position	Peak transmittance	Peak position	Peak transmittance
Structure (a)	494 nm	34.7%	569 nm	45.1%
Structure (b)	502 nm	41%	556 nm	54.4%
Structure (c)	476 nm	40.2%	579 nm	46%
Structure (d)	487 nm	46.7%	555 nm	51.6%

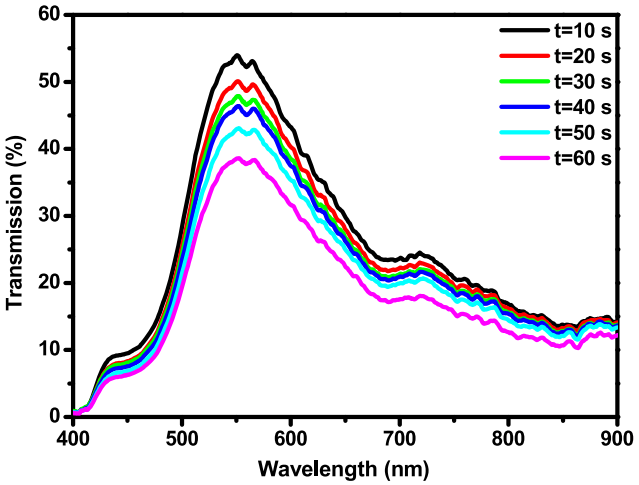

Fig. 6 The evolution of the transmission spectra as a function of time under the UV pump for the Au nanostructures (b)

Figure 6 shows the evolution of the transmission spectra as a function of time under the UV pump for the Au nanostructures (b). We can see that the transmission peak intensity decreases with the increase of the pump time. When the BMAB absorbs UV light, the *trans*-isomer transforms into the *cis*-isomer. The *cis*-isomer affects the host nematic as an impurity, disrupting the local order and forming an isotropic phase. This order change generates a photoinduced refractive index modulation. At the homogenous alignment, the photoresponsive LCs demonstrate a nematic state, as shown in Fig. 2. Although the LC domains are parallel to the substrate, they may rotate within the plane. Statistically, an unpolarized incoming beam will see an average of the ordinary and extraordinary indices. Therefore, the effective refractive index at the nematic state can be written as $n_{\text{nem}} \cong \sqrt{(n_{\text{o}}^2 + n_{\text{e}}^2)/2} = 1.637$. As discussed, the *tans-cis* photoisomerization results in the N–I phase transition of LCs. As pump time increases, more and more BMAB *trans*-isomers transform into *cis*-isomers. The LCs become less and less nematic due to the disruption of long-range order. Ultimately, the LCs approach the isotropic state. At the isotropic state, the effective refractive index becomes $n_{\text{iso}} \cong (2n_{\text{o}} + n_{\text{e}})/3 = 1.596$, a 0.041 decrease in refractive index compared to n_{nem}. As a result, we observed a ~15% decrease in the peak transmission intensity due to photoinduced refractive index modulation. It is worth mentioning that only the LC molecular layer that is near (generally <100 nm) to the Au nanostructures affects the plasmonic properties strongly [4], i.e., the coupling between photons and plasmons. From our experiments, only a slight decrease of refractive index resulted in a significant modulation of transmission intensity. It is therefore expected that the modulation depth could be further enhanced by using a LC with a larger birefringence. We also note that such a hybrid system shows a slow response speed under the UV flood exposure, which may limit its applications. However, in some previous reports, the azo-dye-doped material systems can have a very fast optical response ranging from microseconds to femtoseconds [19, 20]. We believe a faster response speed could be achieved with further optimization of our material formulation.

4 Conclusion

We have fabricated sub-wavelength patterned gold nanostructures on a quartz substrate using FIB technique. By overlaying a photoresponsive LC layer to the gold plasmonic nanostructures, the optical transmission can be further enhanced by more than 10% due to index matching. This hybrid system demonstrates an all-optical modulation of the transmission intensity due to the *trans-cis* photoisomerization-induced N–I phase transition of the LCs. In addition, the all-optical tuning behavior is highly reversible and reproducible. Such a hybrid system can be used for optically switchable color filters.

Acknowledgements This work was financially supported by Agency for Science, Technology, and Research (A*STAR), under the Grant Nos. 0921540099 and 0921540098.

References

1. H. Raether, *Surface Plasmons on Smooth and Tough Surfaces and on Gratings* (Springer, Berlin, 1988)
2. T.W. Ebbesen, H.J. Lezec, H.F. Ghaemi, T. Thio, P.A. Wolff, Extraordinary optical transmission through sub-wavelength hole arrays. Nature **391**, 667–669 (1998)
3. E. Ozbay, Plasmonics: merging photonics and electronics at nanoscale dimensions. Science **311**, 189–193 (2006)

4. Y.J. Liu, Q.Z. Hao, J.S.T. Smalley, J. Liou, I.C. Khoo, T.J. Huang, A frequency-addressed plasmonic switch based on dual-frequency liquid crystals. Appl. Phys. Lett. **97**, 091101 (2010)
5. Y.J. Liu, Y.B. Zheng, J. Liou, I.-K. Chiang, I.C. Khoo, T.J. Huang, All-optical modulation of localized surface plasmon coupling in a hybrid system composed of photo-switchable gratings and Au nanodisk arrays. J. Phys. Chem. C **115**, 7717–7722 (2011)
6. C. Genet, T.W. Ebbesen, Light in tiny holes. Nature **445**, 39–46 (2007)
7. H.S. Lee, Y.T. Yoon, S.S. Lee, S.H. Kim, K.D. Lee, Color filter based on a subwavelength patterned metal grating. Opt. Express **15**, 15457–15463 (2007)
8. E. Laux, C. Genet, T. Skauli, T.W. Ebbesen, Plasmonic photon sorters for spectral and polarimetric imaging. Nat. Photonics **2**, 161–164 (2008)
9. K. Diest, J.A. Dionne, M. Spain, H.A. Atwater, Tunable color filters based on metal-insulator-metal resonators. Nano Lett. **9**, 2579–2583 (2009)
10. T. Xu, Y.-K. Wu, X.G. Luo, L.J. Guo, Plasmonic nanoresonators for high-resolution color filtering and spectral imaging. Nat. Commun. **1**, 59 (2010)
11. E.S.P. Leong, Y.J. Liu, B. Wang, J.H. Teng, Effect of surface morphology on optical properties in metal-dielectric-metal thin film systems. ACS Appl. Mater. Interfaces **3**, 1148–1153 (2011)
12. Y.J. Liu, Y.B. Zheng, J.J. Shi, H. Huang, T.R. Walker, T.J. Huang, Optically switchable gratings based on azo-dye-doped, polymer-dispersed liquid crystals. Opt. Lett. **34**, 2351–2353 (2009)
13. Y.J. Liu, H.T. Dai, X.W. Sun, Holographic fabrication of azo-dye-functionalized photonic structures. J. Mater. Chem. **21**, 2982–2986 (2011)
14. K.G. Yager, C.J. Barrett, Novel photo-switching using azobenzene functional materials. J. Photochem. Photobiol. A, Chem. **182**, 250–261 (2006)
15. A. Mooradian, Photoluminescence of metals. Phys. Rev. Lett. **22**, 185–187 (1969)
16. G.T. Boyd, Z.H. Yu, Y.R. Shen, Photoinduced luminescence from the noble metals and its enhancement on roughened surfaces. Phys. Rev. B **33**, 7923–7936 (1986)
17. M. Xiao, N. Rakov, Surface propagation with a large spectral redshift on a gold thin film containing subwavelength holes. Phys. Lett. A **309**, 452–456 (2003)
18. Y.J. Liu, E.S.P. Leong, B. Wang, J.H. Teng, Optical transmission enhancement and tuning by overlaying liquid crystals on a gold film with patterned nanoholes. Plasmonics **6**, 659–664 (2011)
19. M. Takei, H. Yui, Y. Hirose, T. Sawada, Femtosecond time-resolved spectroscopy of photoisomerization of methyl orange in cyclodextrincs. J. Phys. Chem. A **105**, 11395–11399 (2001)
20. I.C. Khoo, J.-H. Park, J.D. Liou, Theory and experimental studies of all-optical transmission switching in a twist-alignment dye-doped nematic liquid crystal. J. Opt. Soc. Am. B **25**, 1931–1937 (2008)